Article

Cell Reports

Synaptophysin 1 Clears Synaptobrevin 2 from the Presynaptic Active Zone to Prevent Short-Term Depression

Graphical Abstract

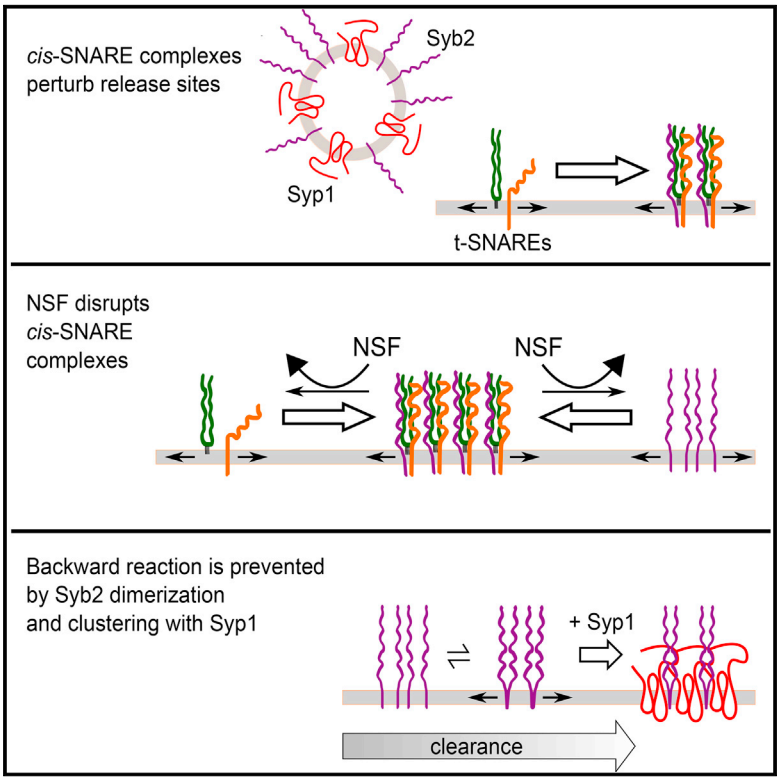

Highlights

- Self-assembly of Syb2 and Syp1 into clusters mediates release site clearance
- Syp1 prevents exocytosed surplus Syb2 from *cis*-SNARE complex formation
- Loss of Syp1 causes strong frequency-dependent short-term depression
- The G100Y mutation of Syb2 has a dominant-negative effect on release site clearance

Authors

Rajit Rajappa, Anne Gauthier-Kemper, Daniel Böning, Jana Hüve, Jürgen Klingauf

Correspondence

klingauf@uni-muenster.de

In Brief

Rajappa et al. identify self-assembly of exocytosed Synaptobrevin 2 and Synaptophysin 1 by homo- and hetero-oligomerization at endocytic zones as a key mechanism mediating release site clearance. Both prevent *cis*-SNARE complex formation at the active zone and ensuing short-term depression.

Rajappa et al., 2016, Cell Reports *14*, 1369–1381
February 16, 2016
http://dx.doi.org/10.1016/j.celrep.2016.01.031

Cell Reports
Article

Synaptophysin 1 Clears Synaptobrevin 2 from the Presynaptic Active Zone to Prevent Short-Term Depression

Rajit Rajappa,[1,3,5] Anne Gauthier-Kemper,[1,5] Daniel Böning,[1] Jana Hüve,[1,2] and Jürgen Klingauf[1,2,4,*]
[1]Department of Cellular Biophysics, Institute of Medical Physics and Biophysics, University of Münster, 48149 Münster, Germany
[2]Fluorescence Microscopy Facility Münster, Center for Nanotechnology, 48149 Münster, Germany
[3]Cells in Motion, International Max Planck Research School Graduate Program, Schlossplatz 5, 48149 Münster, Germany
[4]Cluster of Excellence EXC 1003, Cells in Motion, 48149 Münster, Germany
[5]Co-first author
*Correspondence: klingauf@uni-muenster.de
http://dx.doi.org/10.1016/j.celrep.2016.01.031

SUMMARY

Release site clearance is an important process during synaptic vesicle (SV) recycling. However, little is known about its molecular mechanism. Here we identify self-assembly of exocytosed Synaptobrevin 2 (Syb2) and Synaptophysin 1 (Syp1) by homo- and hetero-oligomerization into clusters as key mechanisms mediating release site clearance for preventing *cis*-SNARE complex formation at the active zone (AZ). In hippocampal neurons from Syp1 knockout mice, neurons expressing a monomeric Syb2 mutant, or after acute block of the ATPase N-ethylmaleimide-sensitive factor (NSF), responsible for *cis*-SNARE complex disassembly, we found strong frequency-dependent short-term depression (STD), whereas retrieval of Syb2 by compensatory endocytosis was only affected weakly. Defects in Syb2 endocytosis were stimulus- and frequency-dependent, indicating that Syp1 is not essential for Syb2 retrieval, but for its efficient clearance upstream of endocytosis. Our findings identify an SV protein as a release site clearance factor.

INTRODUCTION

Fusion of synaptic vesicles (SVs) during synaptic transmission is mediated by soluble N-ethylmaleimide-sensitive factor attachment protein receptor (SNARE) proteins, the v-SNARE Synaptobrevin 2 (Syb2) and the t-SNAREs Syntaxin 1A (Stx1A) and SNAP-25, that form a stable ternary *trans*-SNARE complex via coiled coiling of highly conserved SNARE motifs (Jahn and Scheller, 2006; Söllner et al., 1993a, 1993b). After fusion, the SNARE complexes, now in the *cis* position, need to be disassembled by the ATPase N-ethylmaleimide-sensitive factor (NSF) and α SNAPs (Söllner et al., 1993a, 1993b); otherwise, they would accumulate at the active zone (AZ) and eventually perturb their function. Although Stx1A and SNAP-25 appear to be organized in clusters at sites of release (Sieber et al., 2007), the SV proteins Syb2 and Synaptotagmin 1 (Syt1) are resorted and preassembled in membrane patches, constituting a "readily retrievable pool" (RRetP) for compensatory endocytosis (Wienisch and Klingauf, 2006) outside of the AZ (Hua et al., 2011, 2013). This sorting must involve control of SV protein localization and dynamics during partition from sites of fusion (AZ) to sites of endocytosis (peri-AZ), a process termed "release site clearance" (Neher, 2010; Haucke et al., 2011). Recent studies have demonstrated that impairing endocytosis leads to a rapid form of short-term depression (STD) that is not caused by insufficient SV supply, but is a result of slow clearance of SV components from release sites (Hosoi et al., 2009; Wu et al., 2009; Hua et al., 2013). These findings imply an important role for endocytic proteins in conjunction with scaffold proteins in and around the AZ for maintaining synaptic transmission.

However, SV proteins themselves might facilitate release site clearance. Syb2 constitutes the most abundant SV protein, with approximately 70 copies per SV (Takamori et al., 2006), although only one to three copies per SV are sufficient for fusion (Domanska et al., 2009; Mohrmann et al., 2010; van den Bogaart et al., 2010; Sinha et al., 2011). Syb2 can homodimerize (Calakos and Scheller, 1994; Edelmann et al., 1995) by its transmembrane domain (TMD) (Laage and Langosch, 1997; Roy et al., 2004; Kroch and Fleming, 2006). In addition, it can oligomerize directly with the second most abundant SV protein, Synaptophysin 1 (Syp1) (Calakos and Scheller, 1994; Washbourne et al., 1995; Becher et al., 1999; Khvotchev and Südhof, 2004), which has been suggested to serve as an adaptor for Syb2 endocytosis (Gordon et al., 2011). The Syb2-Syp1 interaction has been shown to inhibit Syb2 from taking part in SNARE complex formation in synaptosomes, leading to the proposal that Syp1 might control the availability of Syb2 to enter SNARE complexes (Edelmann et al., 1995). However, Syp1 knockout (KO) mice reproduce normally and show no overt phenotype (Eshkind and Leube, 1995; McMahon et al., 1996) but display mild behavioral alterations with defects in learning and memory (Schmitt et al., 2009), indicating possible synaptic dysfunction.

Neuronal cultures from cortices of Syp1 KO mice have been reported previously to display almost no retrieval of Syb2 from presynaptic membranes, suggesting that Syp1 may serve as an adaptor protein for Syb2 (Gordon et al., 2011). In contrast, another study shows only delayed endocytosis of several SV proteins upon Syp1 KO (Kwon and Chapman, 2011). In line with this, we observed slightly less efficient Syb2 retrieval in Syp1 KO hippocampal neurons only after strong or prolonged stimulation. However, upstream of Syb2 retrieval, we found that loss of Syp1 induced frequency-dependent STD. Using total internal reflection fluorescence (TIRF)-photoactivation localization microscopy (PALM), we found that Syb2 forms clusters at the plasma membrane (PM). Clustering is increased when Syp1 is present and reduced when Syb2 is not able to dimerize. Using a monomeric Syb2(G100Y) mutant, we found that Syb2 dimerization is also important for release site clearance because synapses expressing Syb2(G100Y) displayed even stronger frequency-dependent STD. Experiments interfering with *cis*-SNARE complex disassembly using the NSF inhibitor N-ethylmaleimide (NEM) indicate that both the ability to dimerize and the interaction with Syp1 are necessary to prevent Syb2 from forming *cis*-SNARE complexes at the AZ and STD. Our data demonstrate the functional role of Syp1 for Syb2 clearance and sequestration into clusters and provide an explanation for the existence of the RRetP outside of the AZ.

RESULTS

Loss of Syp1 Has Only a Minor Effect on Endocytosis of Syb2

Although Syp1 is one of the most abundant SV proteins, its specific role remains elusive. In a recent study using fusion constructs of SV proteins with pHluorin (Miesenböck et al., 1998), a selective blockade of Syb2 retrieval during endocytosis was observed in Syp1 KO mice (Gordon et al., 2011). Taking into account that Syp1 KO mice are viable and show no overt phenotype (Eshkind and Leube, 1995), the drastic effect on Syb2 retrieval seems questionable. Accordingly, a parallel study has shown that endocytosis of SV proteins is not blocked but only slowed down in Syp1 KO mice (Kwon and Chapman, 2011).

Using the same Syp1 KO strain, we repeated analyses of exo-endocytosis of Syb2-pHluorin (SpH) in hippocampal neurons. Fluorescent transients in neurons from Syp1 KO mice were undistinguishable from those from wild-type (WT) mice after 50 action potentials (APs) (Figure 1A, left), but incomplete retrieval was observed after stronger stimulation with 200 APs at 20 Hz, rescued by overexpression of Syp1-mRFP (Figures 1A, right, and 1B). This indicates that the reported defects of Syb2 retrieval might be use-dependent. Similar to recent data (Kwon and Chapman, 2011), we observed reduced Syt1 retrieval upon stimulation with 200 APs at 20 Hz in Syp1 KO mice (Figure S1), indicating that the effect is not limited to Syb2 alone.

To check whether incomplete recovery also depends on frequency, we stimulated at 10 Hz. Indeed, no changes in Syb2 endocytosis kinetics were observed, even with 200 APs (Figures 1C and 1D). Our results are in disagreement with the report of a complete and selective block of Syb2 retrieval (Gordon et al., 2011), although we used the same mouse strain.

Syb2 Displays Strong Frequency-Dependent STD in Syp1 KO Neurons

An incomplete recovery of Syb2 after stimulation could be due to a decreased endocytosis rate, a delayed or incomplete SV acidification downstream of endocytosis, or, alternatively, a defect in exo-endocytic coupling, which has been shown to be essential for proper retrieval of SV components but also for clearing release sites (Hosoi et al., 2009; Wu et al., 2009; Hua et al., 2013; Gauthier-Kemper et al., 2015). Earlier work on hippocampal cultures from Syp1 KO mice already excluded a defect in SV acidification (Kwon and Chapman, 2011). However, the observed frequency dependence of Syb2 recovery (Figure 1) rather hints at a defect in release site clearance of Syb2 than a defect in endocytosis itself. Therefore, we analyzed the pure exocytic SpH responses after stimulation with increasing frequencies in WT neurons, overexpressing Syp1-mRFP, and Syp1 KO neurons in the presence of the vATPase inhibitor Folimycin to mask endocytosis. For quantification of frequency-dependent STD, we used the prepulse normalization protocol we developed earlier (Hua et al., 2013). Neurons were subjected to a pre-test normalization stimulus of 50 APs at 20 Hz. A test stimulus of 200 APs at 5, 20, or 40 Hz was applied 60 s later (Figure 2A). In WT neurons, total fluorescence increases were similar for all frequencies (Figure 2B). This agrees well with the results obtained using rat hippocampal neurons (Hua et al., 2013). Responses from KO neurons, however, showed strong STD at 40 Hz but not at 5 and 20 Hz, which could be rescued by coexpression of Syp1-mRFP (Figures 2C–2E). The observed STD could be due to perturbed release site function caused by improper Syb2 clearance or, alternatively, by reduced availability of SVs; e.g., caused by reduced fusion competence. Therefore, we analyzed SV exocytosis amplitudes after multiple stimulations (50 APs at 20 Hz at 60-s intervals) in the presence of Folimycin to probe SV availability. SVs trapped in the alkaline state after a first round of exo-endocytosis will not contribute further to a fluorescence increase during subsequent stimulation. This leads to a progressive reduction of evoked fluorescence responses (Li et al., 2005; Hua et al., 2013). Fluorescence responses decreased gradually to about 50% of the initial value both in WT and KO neurons (Figures 2F and 2G). Therefore, STD is the result of reduced availability of release sites.

Syb2 Dimerization and the Presence of Syp1 Constitute a First Step for Self-Assembly into Surface Nanodomains

Besides a suggested interaction with AP180/CALM (Koo et al., 2011), self-assembly with other SV proteins might drive the uptake of Syb2 into newborn SVs (Wienisch and Klingauf 2006; Gordon and Cousin, 2014). Syp1 and Syb2 are able to form hetero-oligomers (Calakos and Scheller, 1994; Edelmann et al., 1995; Washbourne et al., 1995). This interaction has been proposed to mediate targeting of Syb2 to SVs (Pennuto et al., 2003), and Syp1 might simply function as an SV-integral adaptor for Syb2 (Gordon and Cousin, 2014). In addition, Syb2 is able to form homodimers by its TMD that can be disrupted by a single

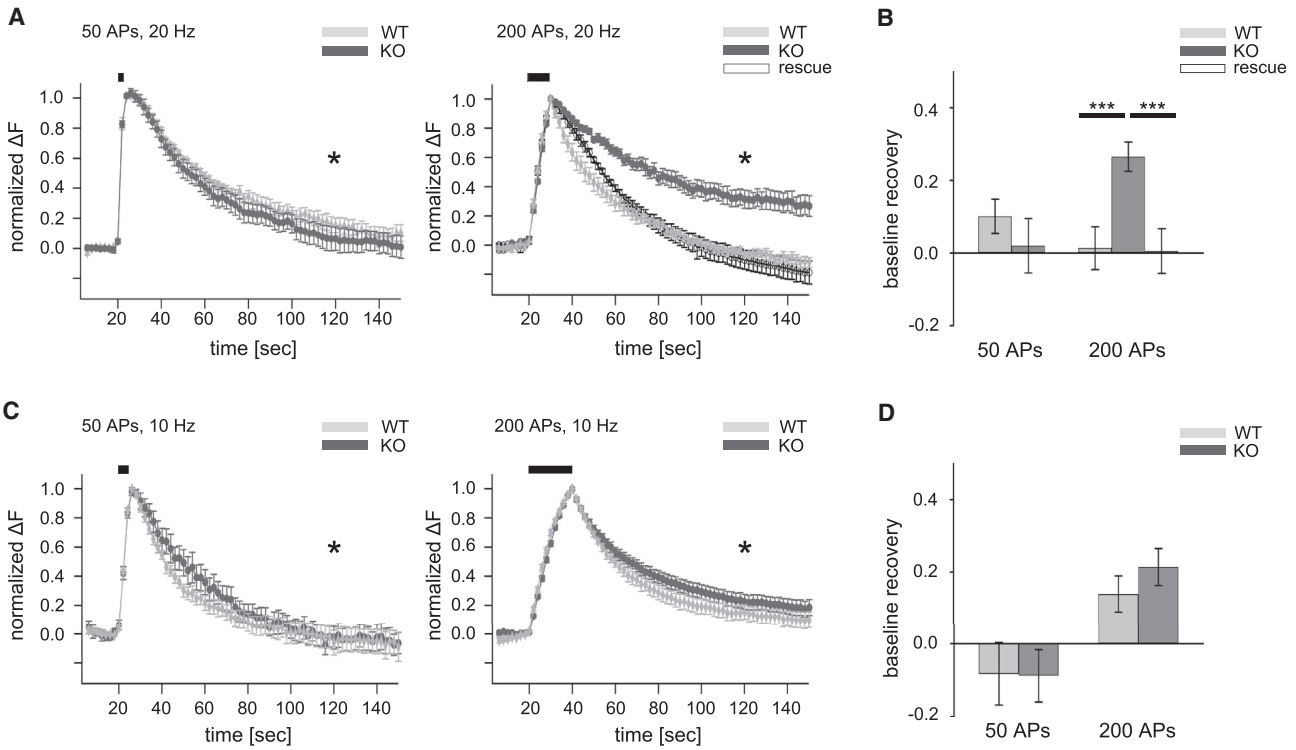

Figure 1. Loss of Syp1 Causes Incomplete Syb2 Retrieval Only at Strong Stimulations

(A) Average fluorescence transients of SpH expressed in hippocampal WT (gray) or Syp1 KO mice (dark gray) after stimulation with 50 APs at 20 Hz (left) or 200 APs at 20 Hz (right). Only at stronger stimulation does loss of Syp1 lead to incomplete retrieval of Syb2, which can be rescued by Syp1-mRFP (right). Errors in SEM, n = 7–18, >50 boutons each.

(B) Quantification of recovery of fluorescence transients from (A). Deviations from baseline 100 s after stimulation are shown (* in A). Errors in SEM, ***p < 0.001, n = 7–18.

(C) Average transients of SpH after 10-Hz stimulation. Again, only after stronger stimulations is retrieval incomplete (right), but no significant difference is seen between WT and Syp1 KO. Errors in SEM, n = 8–10, >50 boutons each.

(D) Quantification of recovery as in (B) of data from (C). Deviations from baseline 100 s after stimulation (* in C) are shown. Errors in SEM, n = 8–10.

See also Figures S1 and S3.

glycine-to-tyrosine mutation (G100Y; Fdez et al., 2010). Disruption of Syb2 dimerization does not negatively influence hetero-oligomerization with Syp1 in pull-down assays with whole-cell lysates of NGF-treated PC12 cells transfected with WT or G100Y-mutated Syb2 fused to pHluorin (Figure S2A). Furthermore, Syb2 WT and Syp1 colocalized close to the membrane periphery in patches (Figure S2B, left), whereas Syb2(G100Y) only partially colocalized with Syp1 (Figure S2B, right) and is mainly absent from the PM region, which indicates a trafficking and/or trapping defect and suggests that the ability of Syb2 to dimerize increases the PM fraction. We further used PC12 cells to perform super-resolution imaging using a combination of TIRF microscopy and PALM to quantitatively analyze the PM fraction of both Syb2 variants. Unfortunately, TIRF-PALM, as used here, is not applicable to neuronal synapses because these are attached to dendrites and oriented in all directions. Even 3D PALM does not have sufficient axial resolution to distinguish between proteins in the peri-AZ membrane and nearby SVs. PC12 cells are derived from the same neuronal precursor cells during development and can develop a neuron-like phenotype with NGF treatment. Moreover, transcriptome profiling comprised about 765 genes, including genes for Syp1 and SNARE proteins (Saminathan et al., 2009). Therefore, they represent a model system closest to neurons for studying PM distribution of Syb2. As a marker, we used the irreversibly photoconvertible dendra2, which displays a comparably low blinking number (Durisic et al., 2014) and is preferably used for protein stoichiometry measurements using single-molecule counting methods (Lee et al., 2012; Renz et al., 2012). However, overcounting still occurs because of repeated blinking after activation.

NGF-treated PC12 cells expressing dendra2 fusion constructs were photoconverted at 405 nm in TIRF illumination, and individual localizations were read out at 561 nm. Reconstructed images show the numbers of localizations per position (color-coded from blue to red) for Syb2 (Figure 3A, top) and Syb2(G100Y) (Figure 3A, bottom). To estimate clustering, k-nearest neighbor (kNN) analysis was performed on regions of interest (ROIs), which displayed homogeneous staining without visible holes or bright aggregates. Measured distances between each molecule and its kNN within the analyzed ROI were normalized by the expected distance for a random distribution without clustering (Poisson distribution) and plotted as a function of kNN.

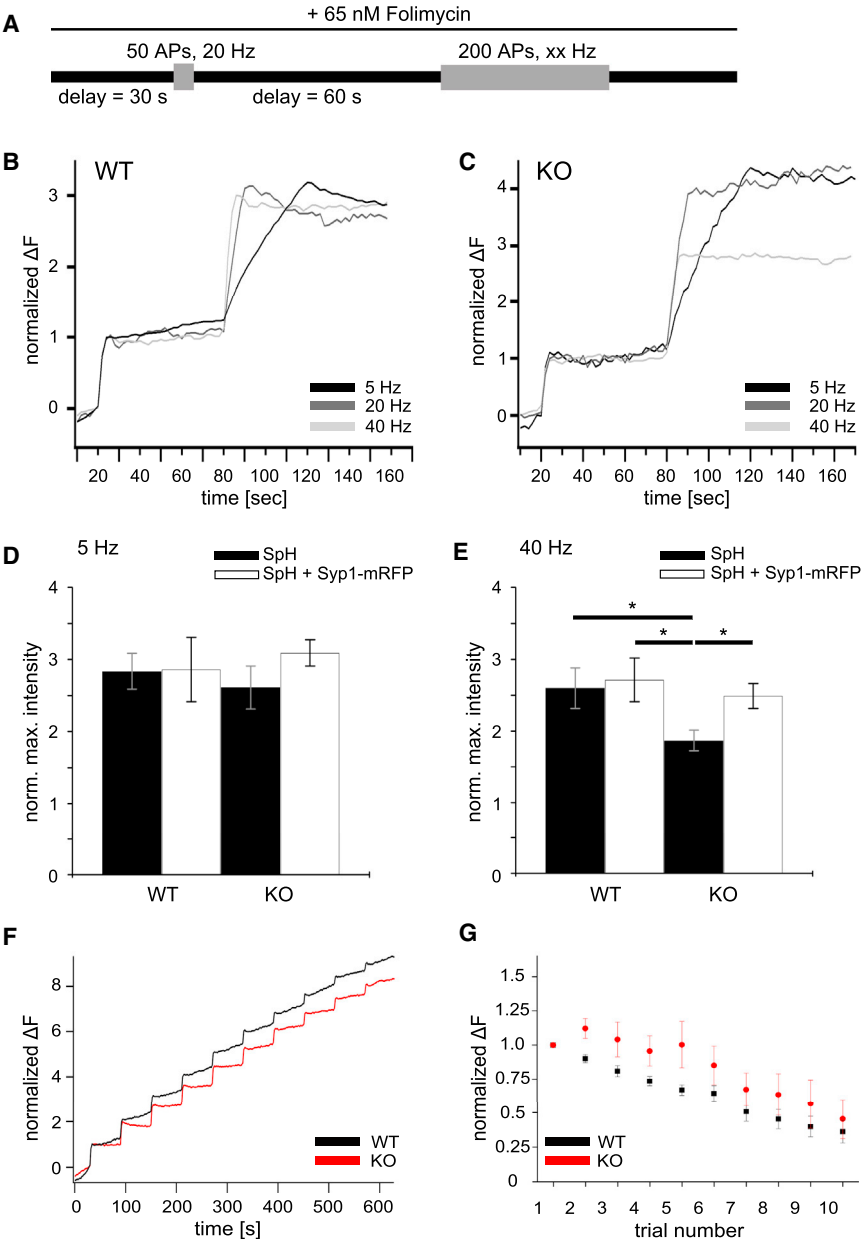

Figure 2. Loss of Syp1 Induces a Frequency-Dependent Release Depression

(A) Schematic of the experimental design. Neurons were stimulated twice in the presence of 65 nM Folimycin. The first stimulus with 50 APs at 20 Hz was used as a calibration stimulus. The second stimulus with 200 APs was applied after 60 s using increasing frequencies (xx = 5, 20, or 40 Hz).

(B) Exemplary fluorescence SpH response in WT neurons to 50 APs at 20 Hz followed by 200 APs at 5 Hz (black), 20 Hz (dark gray), or 40 Hz (light gray) in the presence of Folimycin. Each trace was normalized to the amplitude of the calibration stimulus. No STD was observed.

(C) Exemplary fluorescence SpH response in Syp1 KO neurons. Note the strong STD after stimulation with 40 Hz.

(D) Normalized SpH responses to 5 Hz in WT and Syp1 KO neurons alone (black) or together with Syp1-mRFP (white). Loss of Syp1 leads to only weak STD at low frequencies. Errors in SEM, n = 7–10 experiments, >100 boutons each.

(E) Normalized SpH responses to 40 Hz, leading to significant STD after Syp1 KO (2.6 ± 0.28 for WT and 1.87 ± 0.15 for KO), which could be rescued completely by Syp1-mRFP (2.71 ± 0.3 for WT and 2.49 ± 0.17 for KO). Errors in SEM, *p < 0.05, n = 9–12 experiments, >100 boutons each.

(F) Exemplary SpH responses of WT (black) and Syp1 KO neurons (red) to consecutive stimuli of 50 APs at 20 Hz with 60-s intervals for recovery in the presence of 65 nM Folimycin. Traces are normalized to the first response.

(G) Plot of average fluorescence amplitudes to ten consecutive stimuli from the experiments shown in (F). In the presence of Folimycin, the responses of SpH in WT and KO neurons decrease to 36.15 ± 0.08% and 45.42 ± 0.14%, respectively. Errors in SEM, n = 8–13 experiments, >50 boutons each.

Therefore, a Poisson distribution would result in a normalized distance of 1 to all kNNs (Figure 3A, right, blue dashed line). Syb2 displays a highly reduced distance approximately up to the 100th kNN, indicating clusters of a few ten molecules (results were not corrected for the stochastic numbers of blinks). In comparison, Syb2(G100Y) showed significantly decreased cluster sizes, suggesting that loss of dimerization reduces clustering. To test the role of Syp1 in Syb2 clustering, we repeated the experiments in non-neuronal HEK293 cells, which do not express Syb2, Syp1, or other neuron-specific factors that might influence Syb2 clustering. Cells were transfected with Syb2-dendra2 alone (Figure 3B, top) or together with Syp1-pHluorin (Figure 3B, bottom). kNN analysis revealed that Syp1 enhances clustering of Syb2 (Figure 3B, right).

Taken together, our results indicate that formation of Syb2 surface nanodomains depends on the presence of Syp1 and, circumstantially, on the ability of Syb2 to dimerize. The G100Y mutation significantly reduced Syb2/Syp1 cluster sizes. Therefore, mutant Syb2 might exert a dominant-negative effect by reducing the number of possible protein-protein interactions for clustering.

Dimerization of Syb2 and Coexpression of Syp1 Are Sufficient for Correct Targeting of Syb2 to Neurites

Because we showed that clustering of Syb2 was impaired when Syb2 was monomeric but enhanced when Syp1 was coexpressed, we analyzed the membrane distribution of Syb2 and Syb2(G100Y) in the presence or after acute knockdown (KD) of Syp1. Because our panel of shRNAs against Syp1 caused severe cell death in hippocampal neurons (A.G.K., unpublished data), we used NGF-treated PC12 cells. Coexpression of Syp1 significantly increased the amount of Syb2 in distal neurites compared with the cell body (Figures 4A and 4D, left), whereas Syb2(G100Y) was not

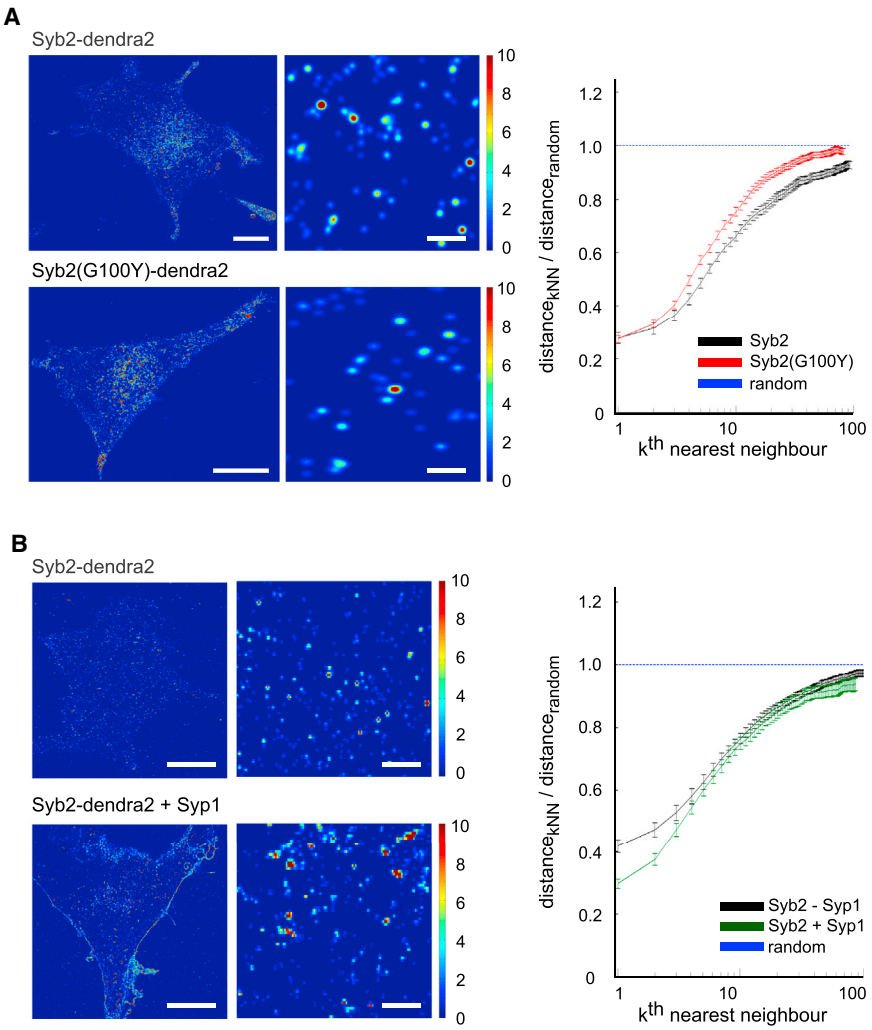

Figure 3. Syb2 Dimerization and the Presence of Syp1 Constitute a First Step for Self-Assembly into Surface Nanodomains

(A) Reconstructed PALM images, magnified regions, and resulting kNN analysis of Syb2-dendra2 (top) and Syb2(G100Y)-dendra2 (bottom) in NGF-treated PC12 cells. The numbers of localizations of molecules are color-coded from blue to red (0 to ≥ 10). Scale bar, 10 μm; magnification, 500 nm. kNN analysis shows distances between the molecules within a selected region that were normalized by the distance between same numbers of molecules in a random distribution. Random distribution is indicated by the dashed blue line. The distribution of Syb2 differs significantly from a random distribution for the first 100 nearest neighbors, indicating clustering of Syb2 molecules in the PM. Clustering is decreased in the case of Syb2(G100Y), which is not able to dimerize. Errors in SEM, n = 6 experiments.

(B) Reconstructed PALM images, magnified regions, and resulting kNN analysis of Syb2-dendra2 in non-neuronal HEK293 cells. Scale bar, 10 μm; magnification, 500 nm. kNN analysis reveals that clustering of Syb2 increases significantly for the first few NN upon Syp1 coexpression, indicating that association with Syp1 enhances clustering of Syb2. Errors in SEM, n = 5–6 experiments.

See also Figure S2.

affected markedly (Figures 4A and 4D, right). This indicates that both Syb2 dimerization and coexpression of Syp1 support targeting of Syb2 to the PM in distal neurites. For Syp1-KD, we used two different stable clonal shRNA lines with different levels of KD, as quantified by western blot (Figure 4C). Expression levels of Syb2 were not affected. Cells expressing scrambled small hairpin RNA (shRNA) showed an increase in Syp1 protein level compared with non-transfected PC12 cells that was in a similar range to Syb2; i.e., the Syp1/Syb2 expression ratio was not changed (1:0.93). Syb2 enrichment in distal neurites observed in Syp1-overexpressing cells was abolished after Syp1-KD but not in cells expressing scrambled shRNA (Figure 4B). In agreement, the ratios of tip to cell body fluorescence showed a reduction after KD similar to that in cells expressing Syb2(G100Y) (Figure 4E). This indicates that Syp1 is required for trafficking and/or targeting of dimerized Syb2 to distal neurites.

Monomeric Syb2 Stranded at the PM Causes Frequency-Dependent STD

Monomeric Syb2(G100Y) might reduce Syb2/Syp1 clustering in a dominant-negative way. Therefore, we analyzed endocytosis kinetics and frequency-dependent STD in Syb2(G100Y)-pHluorin (SpH(G100Y))-expressing hippocampal neurons of WT and Syp1 KO mice. We stimulated the neurons with 50 or 200 APs at 20 Hz. In WT neurons, SpH(G100Y) fluorescence transients fully decayed back to baseline, with kinetics as those observed for SpH (cf. Figure 1A), whereas, in KO neurons, they showed a delay after stronger stimulation with 200 APs, 20 Hz, which could be rescued by Syp1-mRFP (Figure 5A). This shows that dimerization and the degree of Syb2 clustering do not have a major effect on Syb2 retrieval during endocytosis. However, we observed a reduced retrieval of SpH(G100Y) compared with SpH when stimulated at 900 APs at 20 Hz in WT neurons (Figure S3). We next analyzed STD in SpH(G100Y)-expressing WT neurons. Although normalized exocytosis amplitudes were similar for 5- and 20-Hz stimulation, strong STD was observed at 40 Hz (Figure 5B), revealing a dominant-negative effect of SpH(G100Y) on STD. STD was fully rescued by Syp1-mRFP overexpression. To exclude reduced SV availability as a cause, we analyzed synaptic responses to ten consecutive brief stimuli and did not observe any significant differences compared with SpH (Figures 5C and 5D; cf. Figures 2F and 2G). Therefore, Syb2 dimerization is important for fast clearance from release sites on the subsecond timescale but not for retrieval at endocytic sites on the second timescale.

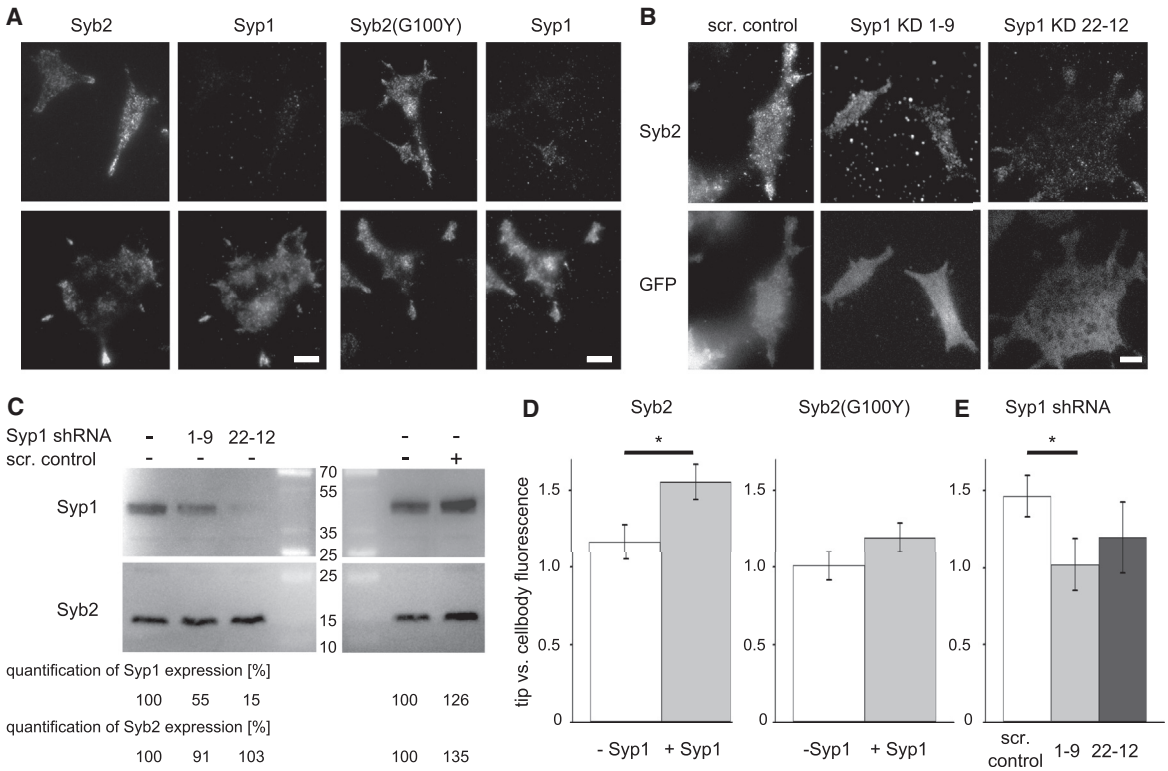

Figure 4. Overexpression of Syp1 Increases Surface Expression of Syb2 but Not Syb2(G100Y) in Distal Neurites of PC12 Cells, and Loss of Syp1 Decreases It

(A) TIRF microscopy images of PC12 cells transfected with SpH (left) or SpH(G100Y) (right) alone or together with Syp1-mRFP. Proteins were detected using antibodies against GFP and Syp1. Coexpression of Syp1 increases expression of Syb2 at distal neurites, whereas Syb2(G100Y) is not affected. Scale bars, 10 μm.

(B) TIRF microscopy images of PC12 cells stably expressing scrambled control shRNA (left) or Syp1 shRNA (center and right). Proteins were detected using Syb2 antibody. Cells expressing shRNAs were selected via a GFP reporter. Upon Syp1 KD, Syb2 is hardly detectable in the PM. Scale bar, 10 μm.

(C) Immunoblots demonstrating shRNA-mediated Syp1 KD in PC12 cells. Two different clonal lines with remaining Syp1 levels of 55% and 15%, respectively, were selected for further experiments (Syp1 KD 1-9, Syp1 KD 22-12). Expression of Syb2 is not affected (91% in sample 1-9 and 103% in sample 22-12 compared with non-transfected cells). Cells expressing scrambled control shRNA show an overall increase in protein expression without affecting the Syp1/Syb2 ratio.

(D) Relative fluorescence intensities of tip-to-cell body expression. Coexpression of Syp1 significantly increases the fluorescence intensity in the tips of Syb2- but not Syb2(G100Y)-expressing PC12 cells. Errors in SEM, *$p < 0.05$, n = 24–37.

(E) Relative fluorescence intensity of tip-to-cell body expression level after KD of Syp1, leading to a reduction of Syb2 expression in the distal tips of PC12 cells. Errors in SEM, *$p < 0.05$, n = 10–30.

Neurons from Syp1 KO Mice or Expressing Monomeric Syb2 Are More Sensitive to the NSF Inhibitor NEM

During SV fusion, neuronal SNARE complexes convert from a *trans* into a *cis* conformation and must be disassembled by the ATPase NSF. Therefore, we wondered whether surface-stranded Syb2 might easily re-form *cis*-SNARE complexes with Stx1A and SNAP-25 highly enriched at sites of release (Sieber et al., 2007; Bar-On et al., 2008) and whether this might be the reason for release site clogging and STD. In other words, might NSF and Syp1 act together in a push-pull mechanism to prevent *cis*-SNARE complex formation between exocytosed Syb2 and abundant t-SNAREs at the AZ? We used increasing amounts of NEM to compete with α-SNAP binding to NSF. Because NEM virtually irreversibly inhibits many proteins by acting on active-site thiol groups, we used acute application. Hippocampal neurons expressing SpH or SpH(G100Y) were stimulated before and 10 min after application of increasing NEM concentrations, and synaptic fluorescence responses were normalized to the total SV pool (unquenched by ammonium chloride) (Figure 6A).

Treatment of neurons with 100 μM NEM did not change endocytosis and re-acidification, although the vATPase is the second most sensitive target for NEM in synaptic boutons (Jouhou et al., 2007). However, we saw a 50% depression in exocytosis amplitude of SpH-expressing WT neurons (half-maximal inhibition [IC_{50}], 100.9 ± 20.7 μM). Upon coexpression of Syp1-mRFP, the IC_{50} value increased (247.7 ± 75.6 μM), whereas Syp1 KO reduced it further (63.5 ± 7.4 μM), which could be rescued by coexpression of Syp1-mRFP (137.4 ± 29.2 μM; Figure 6B). This indicates that Syp1 prevents Syb2 from forming *cis*-SNARE complexes in the PM, most likely by buffering Syb2 in the RRetP at the peri-AZ. In contrast, WT neurons expressing SpH(G100Y) showed a strongly increased NEM sensitivity (IC_{50}, 44.9 ± 8.7 μM). Syp1 KO did not further reduce the IC_{50}

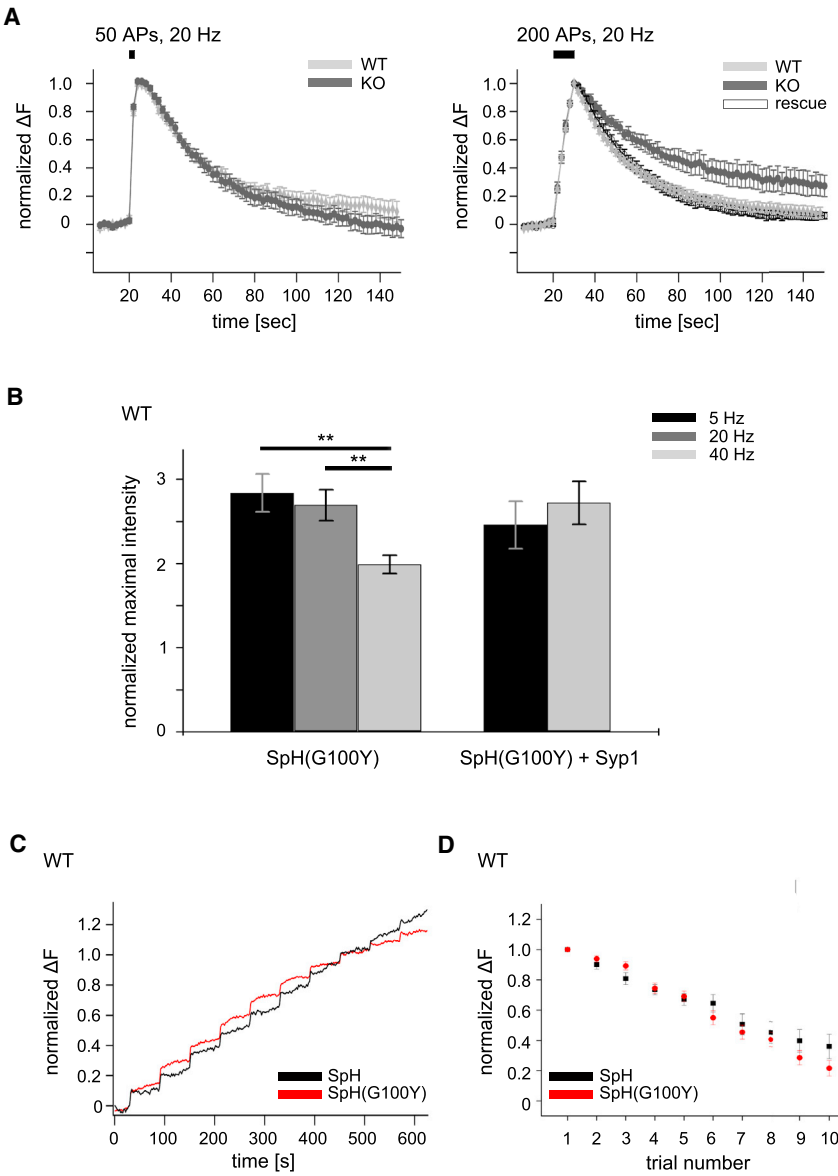

Figure 5. The Syb2(G100Y) Mutation Has a Dominant-Negative Effect on Release Site Clearance

(A) Average SpH(G100Y) transients of WT (gray) and Syp1 KO (dark gray) neurons upon stimulation with 50 APs at 20 Hz (left) or 200 APs at 20 Hz (right). Retrieval is incomplete only after stronger stimulations, which is rescued by coexpression of Syp1-mRFP (right). Errors in SEM, n = 10, >1,000 boutons each.

(B) STD in synaptic boutons of WT and Syp1 KO neurons expressing SpH(G100Y). Shown are fluorescence responses (normalized to calibration responses as in Figure 2) to 5 Hz (black), 20 Hz (dark gray), or 40 Hz (light gray). SpH(G100Y)-expressing neurons are depressed significantly when stimulated at higher frequencies (2.84 ± 0.23 for 5 Hz, 2.69 ± 0.18 for 20 Hz, and 1.99 ± 0.11 for 40 Hz). STD is rescued completely by coexpression of Syp1 (2.46 ± 0.28 for 5 Hz and 2.72 ± 0.26 for 40 Hz). Errors in SEM, **p < 0.01, n = 6–10 experiments, >50 boutons each.

(C) Exemplary SpH (black) and SpH(G100Y) (red) responses to ten consecutive stimuli (50 APs at 20 Hz) as in Figures 2F and 2G.

(D) Plot of average fluorescence amplitudes from (C). The lack of a significant difference between both Syb2 variants indicates that Syb2 dimerization does not affect SV recruitment. Errors in SEM, n = 13–19 experiments, >50 boutons each.

See also Figure S3.

value (51.6 ± 4.0 μM), again pointing out the dominant-negative effect of the G100Y mutation. Overexpression of Syp1-mRFP rescued both the WT and KO (143.3 ± 28.3 μM and 93.4 ± 15.4 μM, respectively; Figure 6C). We conclude that monomeric Syb2 has a higher tendency to form *cis*-SNARE complexes as a consequence of less efficient clustering by Syp1 in the RRetP outside of the AZ. In line with this, changing Syp1 levels is less effective than in SpH-expressing neurons. To check for a frequency-dependent effect of NEM, we analyzed STD in the presence of 30 μM NEM. We saw significant STD upon 40-Hz stimulation that could be rescued by Syp1-mRFP (Figure 6D). Therefore, inhibition by NEM is not only dose- but also frequency-dependent.

Taken together, our results indicate that a combination of two different molecular mechanisms, Syb2 dimerization and Syb2-Syp1 interaction, are important for efficient clearance of Syb2 away from the AZ and buffering in the RRetP at the peri-AZ. We propose that Syp1 primarily serves as a clearance factor, preventing exocytosed surplus Syb2 from *cis*-SNARE complex formation and, therefore, clogging of release sites.

DISCUSSION

Using live cell imaging and super-resolution microscopy, we were able to show that both Syb2 dimerization and the Syb2-Syp1 interaction are essential for efficient clearance of Syb2 from the AZ. We propose that Syp1 primarily serves as a clearance factor, preventing exocytosed Syb2 from *cis*-SNARE complex formation and, thereby, avoiding clogging of release sites (Figure 7).

Functional Role of the Syb2-Syp1 Interaction

We showed that Syp1 increases clustering of Syb2 in the PM. Syp1 overexpression enhanced targeting of Syb2 to distal neurites in PC12 cells, whereas Syp1 KD decreased proper targeting. In agreement with our observation, previous studies have shown that Syp1 efficiently localizes Syb2 to synapses (Pennuto et al., 2003; Wienisch and Klingauf 2006; Bonanomi et al., 2007).

An earlier study (Gordon et al., 2011) has reported that Syb2 endocytosis was blocked completely in Syp1 KO cortical neurons, in conflict with our data. We only observed a partial

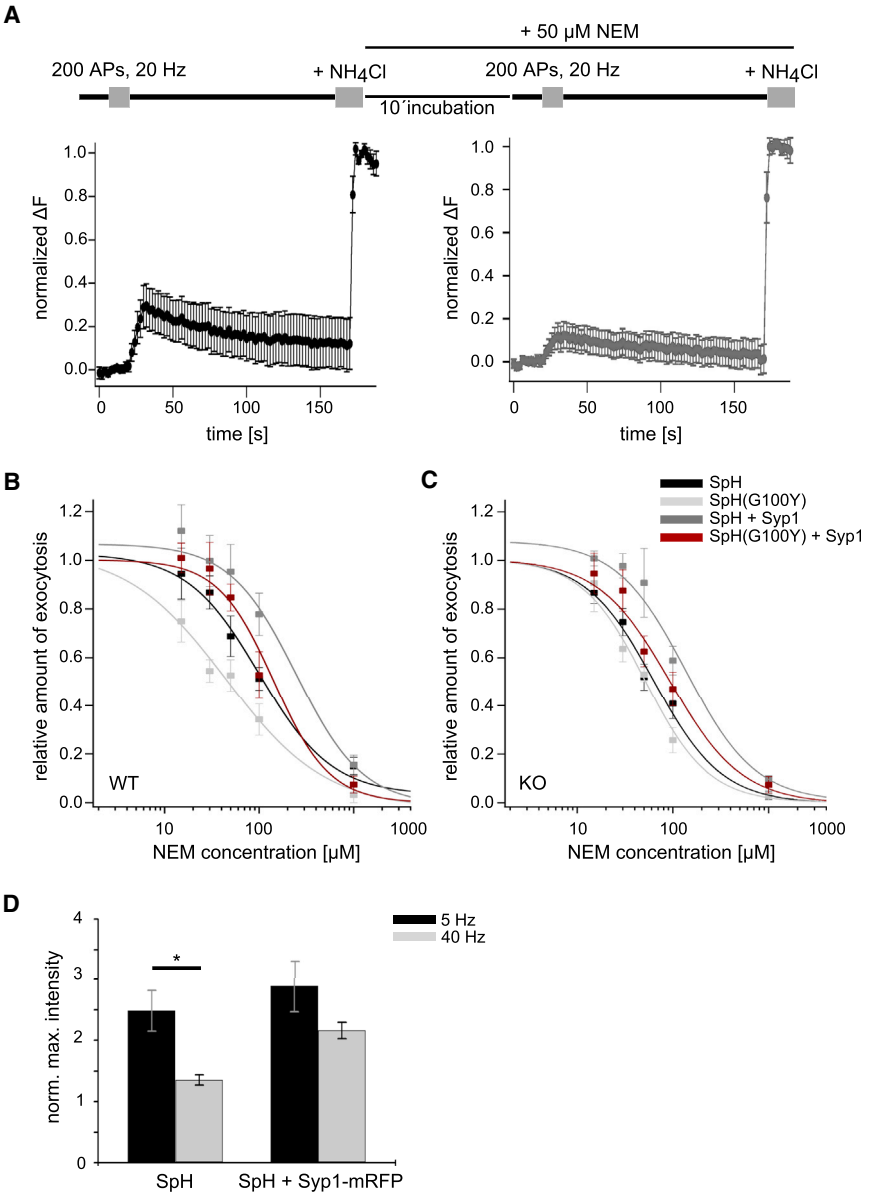

Figure 6. Dimerization and Syp1 Reduce the Sensitivity of Syb2 to the NSF Inhibitor NEM

(A) Experimental design and two exemplary SpH fluorescence transients of WT neurons in response to 200 APs at 20 Hz before and after application of NEM for acute block of NSF. For normalization, an ammonium chloride pulse was given. NEM was applied in different concentrations ranging from 15–1,000 µM. Errors in SD, n > 100 boutons each.

(B and C) Dose-response curves for WT (B) and Syp1 KO (C) neurons. Shown are maximum amplitudes of fluorescence transients for different NEM concentrations relative to the amplitude prior to NEM treatment. Neurons expressed SpH (black) or SpH(G100Y) (light gray) alone or together with Syp1-mRFP (gray for SpH and red for SpH(G100Y), respectively). For calculation of IC_{50} values (see text), data were fit with Hill's equation,

$$F = a - \frac{a-b}{1+\left(\frac{K}{[c]}\right)^{n}},$$

where F is the measured fluorescence amplitude (exocytosis) relative to the control, a and b are the maximum and minimum values, K is the ligand concentration [c] producing IC50, and n is the Hill coefficient. Fitting was done with the Levenberg-Marquardt algorithm. Data points were weighted with their errors. Errors in SEM, n = 5–16 experiments, >50 boutons each.

(D) STD of WT neurons expressing SpH in the presence of 30 µM NEM. In contrast to untreated neurons (Figure 2), weak STD is already observed at 5 Hz (black) and very strong STD at 40 Hz (gray) (2.48 ± 0.33 for 5 Hz and 1.35 ± 0.09 for 40 Hz) and can be rescued by coexpression of Syp1 (2.89 ± 0.42 for 5 Hz and 2.16 ± 0.14 for 40 Hz). Errors in SEM, *p < 0.05, n = 5–10 experiments, >80 boutons each

reduction in Syb2 endocytosis under similar stimulation conditions, although we used the same KO strain. However, a complete block of Syb2 endocytosis and, therefore, retrieval into SVs surely should have led to the same lethal phenotype as that reported for Syb2 KO mice (Schoch et al., 2001). In part, different requirements for Syp1 in different neuron types may account for the divergent results. Although no other direct interaction of Syp1 with any other SV protein than Syb2 has been observed in neurons, loss of hetero-oligomerization upon Syp1 KO also affects retrieval of other SV proteins, like Syt1 (Figure S1). This observation was consistent with another parallel study in which endocytosis of SV protein 2A (SV2A) and Syt1 was partially blocked upon Syp1 KO under similar stimulation conditions (Kwon and Chapman, 2011). Moreover, at mild stimulation kinetics of Syb2, endocytosis remained unchanged in Syp1 KO neurons, indicating that Syp1 does not play a direct role in Syb2 endocytosis. These findings corroborate our notion that the mild endocytosis defect observed for increasing stimulus strength and frequency is a mere consequence of ineffective release site clearance upstream of endocytosis. Our results demonstrate that improper clearance of exocytosed SpH in Syp1 KO neurons can cause a functional block of previously used release sites, leading to release depression. Our data implicate self-assembly in release site clearance and functionally link release site clearance to the existence of the RRetP at the peri-AZ. Supporting our conclusion, we performed Monte Carlo simulations (2D random walk) of diffusional clearance of Syb2 from the AZ in the presence or absence of a "trapping" RRetP around the AZ to show how the existence of the RRetP at the peri-AZ ("sink") positioned adjacent to sites of fusion at the AZ ("source") facilitates the diffusional clearance from the source (Figure 7B). In both scenarios (i.e., with and without sink), particles diffuse freely but are trapped during their random walk in the presence of the sink, which prevents a random walk back to the source. This

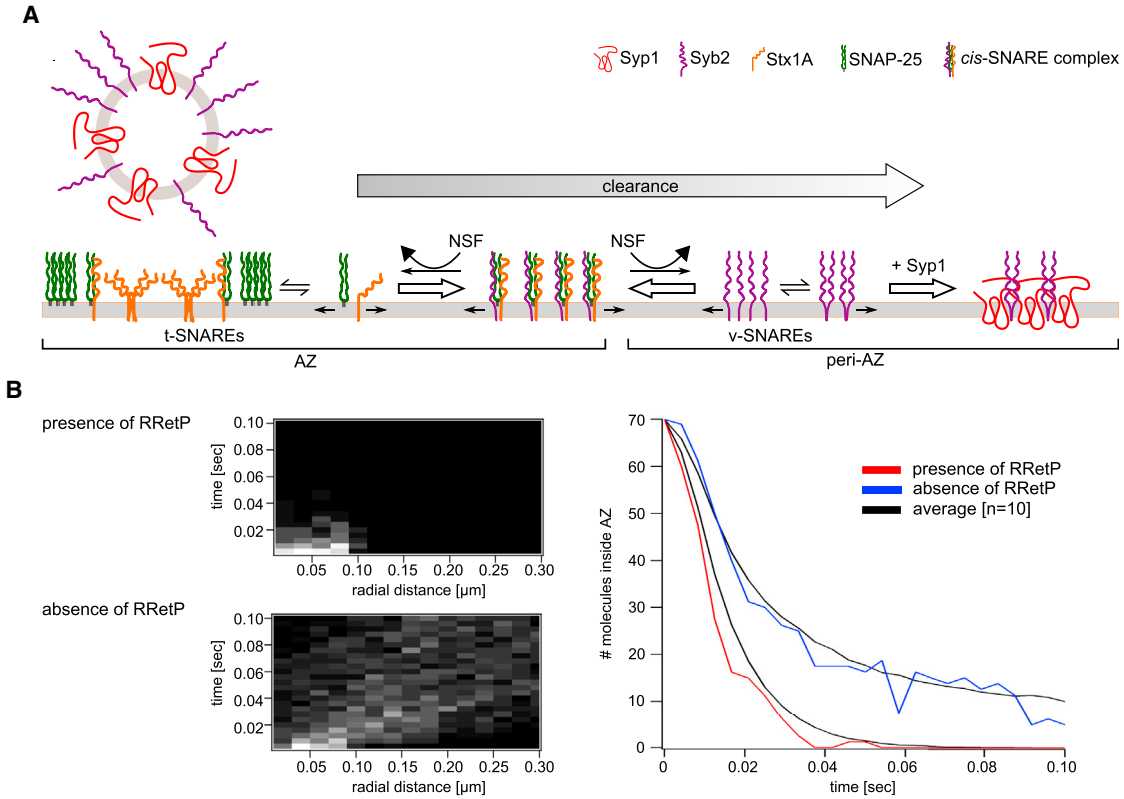

Figure 7. NSF and Syp1 Act in a Push-Pull Mechanism for Release Site Clearance

(A) For release site clearance, Syb2 is pushed away by NSF, which disassembles *cis*-SNARE complexes, and pulled by Syp1, which clusters Syb2 dimers outside of the AZ in the RRetP. Loss of either one leads to accumulation of *cis*-SNARE complexes at sites of SV fusion, thereby perturbing its function, which results in STD. Syb2-Syp1 clusters in the RRetP and t-SNARE clusters form stable domains in the AZ, thereby maintaining its integrity, whereas all other components diffuse freely (arrows in the PM).

(B) Monte Carlo simulations (2D random walk) of diffusional clearance of Syb2 from the AZ in the presence and absence of a trapping RRetP around the AZ. Left: kymographs of the radial positions of 70 Syb2 molecules released by one SV at the center of a circular AZ (200-nm diameter) at time 0 s with a static absorbing RRetP around the AZ (top) or no RRetP (bottom). Molecules diffuse with 0.5 $\mu m^2/s$, as determined experimentally by fluorescence recovery after photobleaching (FRAP) measurements in the axonal PM (J.K., unpublished data). Right: clearance curves (quantification of the kymographs is shown on the left). Absolute numbers of Syb2 molecules within the 200-nm AZ are represented as a function of time. In the presence of an RRetP (red), as many molecules are cleared after 25 ms (corresponding to 40 Hz) as after 100 ms (10 Hz) in the absence of the RRetP (blue). Black clearance curves represent averages of ten simulations each.

also explains the frequency dependence. With or without the sink, particles eventually diffuse away; i.e., distribute in the whole bouton membrane, which is large compared with the AZ area. But with a nearby sink, the process of dilution or clearance is accelerated. At low release frequencies, this slowed clearance does not matter, but at higher frequencies, the existence of the RRetP facilitates clearance (Figure 7A).

Role of Syp1 and Isoforms in Other Preparations

STD as result of a clearance defect has been first reported at the calyx of Held preparation (Hosoi et al., 2009; Wu et al., 2009). At this synapse, 1 mM NEM resulted in a strong decline of the paired pulse ratio only for short inter-stimulus intervals but did not affect overall refilling kinetics of the readily releasable SV pool (Sakaba and Neher, 2003). Therefore, NSF acts downstream of SV fusion and also appears to be important for release site clearance at the calyx. Therefore, we started postsynaptic recordings on calyx of Held preparations of Syp1 KO mice. So far, we were only able to see mild differences in depression (R.R. and H. Taschenberger, unpublished data). However, postsynaptic AMPAR desensitization at very high stimulus frequencies might be a confounding factor. Postsynaptic electrophysiological recordings in hippocampal neurons would be additionally compromised by the severe space-clamp problem. Therefore, we preferred the pHluorin-based prepulse normalization protocol for probing frequency-dependent STD (Hua et al., 2013) in hippocampal neurons. We showed that pHluorin measurements involving transfection as well as measurements with the styryl dye FM1-43 yield identical results, providing direct and linear readouts of presynaptic release, unlike postsynaptic recordings (Hua et al., 2013). Redundancy of Syp1 function by other Syp isoforms, namely Synaptophysin 2, Pantophysin, and Synaptogyrins (Fykse et al., 1993; Haass et al., 1996), may also lead to mild differences. Further experiments are needed for clarification. In the hippocampus, Synaptophysin 2 is highly expressed in granule cells and, to a lesser extent, in CA3

pyramidal cells (Singec et al., 2002). Because both cell types are present in our cultures, an even stronger STD is expected for a double KO. Interestingly, bipolar retinal cells are found to not express Synaptophysin 2 and have been observed to have a reduced number of SVs upon Syp1 KO (Spiwoks-Becker et al., 2001). Moreover, the *Drosophila* genome lacks a Syp homolog and encodes only a single Synaptogyrin isoform. Synaptogyrin-null mutant larval neuromuscular junctions revealed abnormal SV biogenesis and decreased release probability, resulting in increased initial facilitation followed by pronounced depression during tetanic stimulation at 20 Hz (Stevens et al., 2012). Unfortunately, higher frequencies were not tested. However, the *Drosophila* temperature-sensitive NSF mutant *comatose* revealed strong depression (Kawasaki and Ordway, 2009).

cis-SNARE Complex Formation

Disassembly of *cis*-SNARE complexes by NSF is thought to occur after SV exocytosis to allow Syb2 recycling (Jahn and Scheller, 2006). However, in squid giant synapses, flash photolysis of an NSF-inhibiting caged peptide caused rapid release depression after few APs, not depleting SVs (Kuner et al., 2008), which led the authors to argue that SNARE disassembly must occur upstream of docking and priming. In this study, we also observed strong STD when inhibiting NSF with NEM (Figure 6). Our results therefore can reconcile the squid data by showing that a failure in *cis*-SNARE complex dissociation downstream of fusion can perturb release site function. NEM concentrations higher than 0.5 mM have been observed previously to block v-ATPase function (Jouhou et al., 2007). In chromaffin cells, NEM did not affect the initial burst of exocytotic events when used at 0.5–1 mM with an incubation time of 5–10 min (Xu et al., 1999). 1 mM NEM has also been shown to have no effect on SV recruitment in the calyx of Held (Sakaba and Neher, 2003). Therefore, NEM at lower concentration and on a timescale of up to 10 min can be used as an acute blocker of NSF. We observed that Syp1 KO neurons were more sensitive to NEM compared with WT neurons, which could be rescued by Syp1 expression. This increased sensitivity suggests that, in KO neurons, enhanced NSF function partially compensates for the loss of Syb2 clearance. Remarkably, a single point mutation of Syb2, only disrupting its dimerization, rendered synapses most sensitive to NEM (Figures 6B and 6C). Again, this effect could be partially rescued by Syp1 coexpression. In general, we found that Syp1 changed NEM susceptibility in a dose-dependent manner, which might explain the high copy number of Syp1 in SVs. We suggest that RRetP formation outside of the AZ is crucial for preventing the energetically highly favored *cis*-SNARE complex formation by t- and v-SNAREs, which are highly abundant in the synaptic PM, by segregating them into two distinct membrane domains. In PC12 cell membranes, the two t-SNAREs Stx1A and SNAP-25 have been shown to form extended clusters (Sieber et al., 2007) and to spontaneously form stable *cis*-SNARE complexes with free Syb2 (Bar-On et al., 2008). Interestingly, in chromaffin cells, NEM substantially inhibited a second exocytosis burst but not the initial one (Xu et al., 1999). Because secretory granules, unlike SVs, are not reformed from the PM, this finding cannot be explained by SNARE complex disassembly upstream of fusion, as suggested by the fast depression after NSF block in squid giant synapses (Kuner et al., 2008). Likewise, in the calyx of Held, NEM strongly decreased the paired pulse ratio selectively for short inter-stimulus intervals without affecting overall SV recruitment kinetics (Sakaba and Neher, 2003). The most likely explanation is that the large amounts of Syb2 released during the first burst form *cis*-SNARE complexes with abundant t-SNAREs, leading to clogging of release sites. These and our data suggest that clustering of both t- and v-SNAREs in spatially distinct membrane domains (AZ and RRetP at the peri-AZ) work as a mechanism to prevent *cis*-SNARE complex formation at the AZ. In line with this, we have shown that induction of STD by blocking endocytosis is associated with an accumulation of SV proteins in the AZ, probably because of saturation of the RRetP capacity (Hua et al., 2013). Conversely, in the *Drosophila* temperature-sensitive NSF mutant *comatose*, strong depression was accompanied by redistribution of t-SNAREs away from the AZ (Kawasaki and Ordway, 2009). This shows that *cis*-SNARE complex formation indeed leads to disintegration of release sites, resulting in STD. Previous studies have shown that Syb2 bound to Syp1 was not able to participate in SNARE complex formation (Edelmann et al., 1995). Taken together, our results identify dimerization of Syb2 followed by Syp1-mediated clustering and sequestration into the RretP as first important steps in release site clearance. We propose that Syp1 acts downstream of exocytosis and upstream of endocytosis as a clearance factor for Syb2, thereby also enhancing its efficient sorting into newly endocytosed SVs. Because we have shown previously that presorting and preassembly of SV proteins into the RRetP does not highly speed up their endocytic retrieval, we propose that the main function of the RRetP is facilitation of release site clearance.

EXPERIMENTAL PROCEDURES

Plasmid Constructs

Eukaryotic expression plasmids encoding superecliptic pHluorin-Synaptobrevin 2 (SpH), Synaptophysin 1-pHluorin, and Synaptophysin 1-mRFP were generated as described by Wienisch and Klingauf (2006). The eukaryotic expression plasmid for Syb2, fused carboxy-terminally to dendra2, was constructed in pRc/cytomegalovirus (CMV)-based expression vector pDendra2 (Takara Bio). To produce monomeric Syb2, glycine 100 was mutated to tyrosine by site-directed mutagenesis of the respective codon using a site-directed mutagenesis kit (Stratagene/Agilent Technologies). All sequences were verified by DNA sequencing.

Cell Culture and Transfection

PC12 cells were cultured in serum DMEM as described previously (Gauthier-Kemper et al., 2012). Undifferentiated cells were plated on 24-mm poly-D-lysine (PDL)- and collagen-coated glass coverslips (Karl Hecht) at 10^3 cells/cm^2 and cultured in DMEM with 1% (v/v) serum. Cells were flattened by addition of 100 ng/ml rat NGF for 1–2 days. HEK293 cells were cultured in minimal essential medium (MEM) supplemented with 10% (v/v) fetal calf serum (FCS), 2 mM Glutamine, and 1% (v/v) penicillin/streptomycin (stock solution, 10,000 U/ml penicillin and 10 mg/ml streptomycin). For imaging, cells were plated on 24-mm PDL-coated glass coverslips.

Transfections of PC12 and HEK293 cells were performed with Lipofectamine 2000 (Invitrogen) as described previously (Gauthier-Kemper et al., 2012). Electroporation of PC12 cells was performed with the Neon transfection system (Invitrogen). Analysis was carried out 3 days after transfection.

Primary cultures were prepared from newborn (post-natal day 0 [P0]) C57/BL6 WT mice or homozygous Syp1 KO mice as described previously (Wienisch and Klingauf, 2006). Syp1 KO mice were obtained from Prof. Dr. Rudolf Leube (Rheinisch-Westfälische Technische Hochschule [RWTH] Aachen University). All animals were treated in accordance with the regulations and guidelines of the State of North Rhine-Westphalia. Cultures were maintained in Neurobasal medium supplemented with 2% (v/v) B27 (Gibco), 2 mM Glutamine, and 0.1% (v/v) penicillin/streptomycin. At 2 days in vitro (DIV), cells were additionally treated with 1 μM cytosine β-D-arabinofuranoside (Ara-C) to inhibit glial proliferation. Neurons were grown on Matrigel-covered glass coverslips and transfected at 5 DIV by a modified calcium phosphate transfection protocol (Threadgill et al., 1997). Microscopy was performed at 17–21 DIV.

Epifluorescence Microscopy of Living Neurons and Data Analysis

Experiments were carried out in modified Tyrode's solution (140 mM NaCl, 4 mM KCl, 2 mM $CaCl_2$, 1 mM $MgCl_2$, 10 mM glucose, 10 mM HEPES [pH 7.4]; ~310 mOsm). APs were elicited by electric field stimulation (platinum electrodes, 10-mm spacing, 1-ms pulses of 50 mA, and alternating polarity at 20 Hz) applied by constant current stimulus isolator (WPI A 385, World Precision Instruments). 10 μM 6-cyano-7-nitroquinoxaline-2,3-dione (CNQX, Tocris Bioscience) and 50 μM D,L-2-amino-5-phosphonovaleric acid (AP5, Tocris Bioscience) were added to prevent recurrent activity. Fast solution exchanges were achieved through a three-barrel glass tubing perfusion system controlled by a piezo-controlled stepper device (SF778, Warner Instruments). Ammonium chloride solution (pH 7.4) was prepared by replacing 50 mM NaCl with NH_4Cl. Folimycin (Calbiochem) was used at a concentration of 65 nM. The experiments were conducted at room temperature (RT) on an inverted Zeiss 100 microscope equipped with a ×63, numerical aperture (NA) 1.2 water immersion objective. Images were acquired at 0.5 Hz with a cooled charge-coupled device (CCD) camera (Sensicam QE, PCO) controlled by TILLVisION software (Till Photonics) in 2 × 2 binning mode, resulting in 688 × 520 pixels. PHluorin fusion constructs were excited at 480 nm with a computer-controlled monochromator (Polychrom II, Till Photonics). Fluorescence was detected after passing a fluorescein isothiocyanate (FITC)/Cy5 dual-band filter set (AHF Analysentechnik). For dual-color recordings, alternating images in green and red channels were acquired at 0.5 Hz. NEM was dissolved in Tyrode's solution to the respective concentration. Neurons were stimulated with 200 APs at 20Hz. Ammonium chloride solution was perfused for 160 s after stimulation. After washing three times with Tyrode's solution, NEM buffer solution of the required concentration was added. Upon 10-min incubation at RT, the same set of stimulation paradigms was performed in the same region. Quantitative analysis was performed with self-written macros in Igor Pro-6.12 (Wavemetrics) as described previously (Wienisch and Klingauf, 2006). Only experiments containing more than 50 active boutons were considered for analysis.

TIRF-PALM Imaging and Cluster Analysis

For cluster analysis using TIRF-PALM, HEK293 or NGF-treated PC12 cells were fixed 3 days after transfection using 4% paraformaldehyde + 0.2% glutaraldehyde (SERVA Electrophoresis) in PBS for 15 min at 4°C, followed by 30 min at RT. Quenching was done with 0.1 M glycine for 15 min. Cells were finally washed three times with PBS. TIRF-PALM imaging was performed on an inverted Nikon Ti Eclipse microscope equipped with fiber-coupled lasers of different wavelengths (405 nm [60 mW Jive, Cobolt], 488 nm [200 mW Jive, Cobolt], and 561 nm [150 mW Phoxx, Omicron]) controlled by a laser box (Omicron Laserage). Fluorescence emission was detected using a ×100 oil objective (Nikon Apo TIRF, NA 1.46) together with an ORCA Flash complementary metal oxide semiconductor (CMOS) camera (Hamamatsu). Twenty thousand images were taken at an exposure time of 100 ms. Activation of dendra2 was performed with 405 nm at very low laser power (microwatt) and excitation with 561 nm with maximum power. For drift correction, 200-nm tetraspec fluorescence beads (Invitrogen) were added prior to imaging. Single-molecule localization and reconstruction of PALM images were done using QuickPALM software (Henriques et al., 2010), which includes a high-speed reconstruction algorithm using the classical Högbom "CLEAN" method for spot finding, followed by a modified center of mass algorithm to compute the spot position and parameters defining spot shape along the horizontal axis. Drift correction was done by subtraction of the trace of the corresponding tetraspec bead from the traces of each localized spot in the reconstruction using a self-written MATLAB (MathWorks) script. Corrected reconstructed PALM images were plotted as a color code from blue to red. Cluster analysis was done in MATLAB from sections of the cell approximately 2 μm^2 in size using kNN analysis. The results were plotted as a function of the calculated distance between two molecules within the analyzed section divided by the distance between two randomly distributed molecules in the same section. Therefore, a random distribution would lead to a kNN distance of 1 (blue dashed line in the plots).

shRNA-Mediated Downregulation of Syp1

Stable, clonal lines of Syp1-downregulated PC12 cells were generated using different types of shRNA coding sequences for mouse Syp1 (OriGene) according to the manufacturer's protocol (for further details, see Supplemental Experimental Procedures). For immunofluorescence analysis, cells were fixed with 4% (w/v) paraformaldehyde in PBS for 20 min. After washing, cells were quenched with 0.1 M glycine for 20 min and permeabilized for 5 min with 0.2% (v/v) Triton X-100 in PBS. Cells were stained with the respective antibodies diluted in PBS containing 1% (w/v) BSA at RT (2 hr for primary antibodies and 1 hr for secondary antibodies). Coverslips were mounted in PBS. Images were taken using TIRF microscopy performed on a Nikon Ti Eclipse using fiber-coupled lasers of different wavelengths: 491 nm (100 mW Calypso, Cobolt) and 561 nm (100 mW Jive, Cobolt). Fluorescence emission was detected using a ×100 oil objective (Nikon Apo TIRF, NA 1.49) together with an electron-multiplying CCD camera (Andor Technology).

Other Methods

Statistical analysis among experimental groups was performed using paired Student's t test (Origin 7.0) or ANOVA followed by a post hoc Bonferroni test. p Values were as follows: $^*p < 0.05$, $^{**}p < 0.01$, and $^{***}p < 0.001$. Monte Carlo simulations of a 2D random walk of released SV proteins were performed with self-written macros in Igor Pro 6.12 (Wavemetrics) using the built-in random number generator.

SUPPLEMENTAL INFORMATION

Supplemental Information includes Supplemental Experimental Procedures and three figures and can be found with this article online at http://dx.doi.org/10.1016/j.celrep.2016.01.031.

AUTHOR CONTRIBUTIONS

R.R., A.G.K., and J.K. designed the experiments and R.R. and A.G.K. conducted the experiments. D.B. programmed the kNN analysis software, and J.K. programmed the Monte Carlo simulation software. J.H. performed confocal imaging. A.G.K., R.R., and J.K. wrote the paper.

ACKNOWLEDGMENTS

We thank Dr. R. Leube (RWTH Aachen University), for generously providing the Syp1 KO mice, Dr. C.S. Thiel and Dr. M. Wiemhöfer for participation during the early phase of the project, K. Tkotz and K. Zerf for technical assistance, and Dr. M. Kahms for critically reading the manuscript. J.K. was supported by grants from the DFG (ESF Euromembrane, SFB 629, SFB 944, and DFG EXC 1003, Cells in Motion Cluster of Excellence, Münster, Germany).

Received: July 24, 2015
Revised: October 23, 2015
Accepted: January 6, 2016
Published: February 4, 2016

REFERENCES

Bar-On, D., Winter, U., Nachliel, E., Gutman, M., Fasshauer, D., Lang, T., and Ashery, U. (2008). Imaging the assembly and disassembly kinetics of cis-SNARE complexes on native plasma membranes. FEBS Lett. *582*, 3563–3568.

Becher, A., Drenckhahn, A., Pahner, I., Margittai, M., Jahn, R., and Ahnert-Hilger, G. (1999). The synaptophysin-synaptobrevin complex: a hallmark of synaptic vesicle maturation. J. Neurosci. *19*, 1922–1931.

Bonanomi, D., Rusconi, L., Colombo, C.A., Benfenati, F., and Valtorta, F. (2007). Synaptophysin I selectively specifies the exocytic pathway of synaptobrevin 2/VAMP2. Biochem. J. *404*, 525–534.

Calakos, N., and Scheller, R.H. (1994). Vesicle-associated membrane protein and synaptophysin are associated on the synaptic vesicle. J. Biol. Chem. *269*, 24534–24537.

Domanska, M.K., Kiessling, V., Stein, A., Fasshauer, D., and Tamm, L.K. (2009). Single vesicle millisecond fusion kinetics reveals number of SNARE complexes optimal for fast SNARE-mediated membrane fusion. J. Biol. Chem. *284*, 32158–32166.

Durisic, N., Laparra-Cuervo, L., Sandoval-Álvarez, A., Borbely, J.S., and Lakadamyali, M. (2014). Single-molecule evaluation of fluorescent protein photoactivation efficiency using an in vivo nanotemplate. Nat. Methods *11*, 156–162.

Edelmann, L., Hanson, P.I., Chapman, E.R., and Jahn, R. (1995). Synaptobrevin binding to synaptophysin: a potential mechanism for controlling the exocytotic fusion machine. EMBO J. *14*, 224–231.

Eshkind, L.G., and Leube, R.E. (1995). Mice lacking synaptophysin reproduce and form typical synaptic vesicles. Cell Tissue Res. *282*, 423–433.

Fdez, E., Martínez-Salvador, M., Beard, M., Woodman, P., and Hilfiker, S. (2010). Transmembrane-domain determinants for SNARE-mediated membrane fusion. J. Cell Sci. *123*, 2473–2480.

Fykse, E.M., Takei, K., Walch-Solimena, C., Geppert, M., Jahn, R., De Camilli, P., and Südhof, T.C. (1993). Relative properties and localizations of synaptic vesicle protein isoforms: the case of the synaptophysins. J. Neurosci. *13*, 4997–5007.

Gauthier-Kemper, A., Weissmann, C., Reyher, H.J., and Brandt, R. (2012). Monitoring cytoskeletal dynamics in living neurons using fluorescence photoactivation. Methods Enzymol. *505*, 3–21.

Gauthier-Kemper, A., Kahms, M., and Klingauf, J. (2015). Restoring synaptic vesicles during compensatory endocytosis. Essays Biochem. *57*, 121–134.

Gordon, S.L., and Cousin, M.A. (2014). The Sybtraps: control of synaptobrevin traffic by synaptophysin, α-synuclein and AP-180. Traffic *15*, 245–254.

Gordon, S.L., Leube, R.E., and Cousin, M.A. (2011). Synaptophysin is required for synaptobrevin retrieval during synaptic vesicle endocytosis. J. Neurosci. *31*, 14032–14036.

Haass, N.K., Kartenbeck, M.A., and Leube, R.E. (1996). Pantophysin is a ubiquitously expressed synaptophysin homologue and defines constitutive transport vesicles. J. Cell Biol. *134*, 731–746.

Haucke, V., Neher, E., and Sigrist, S.J. (2011). Protein scaffolds in the coupling of synaptic exocytosis and endocytosis. Nat. Rev. Neurosci. *12*, 127–138.

Henriques, R., Lelek, M., Fornasiero, E.F., Valtorta, F., Zimmer, C., and Mhlanga, M.M. (2010). QuickPALM: 3D real-time photoactivation nanoscopy image processing in ImageJ. Nat. Methods *7*, 339–340.

Hosoi, N., Holt, M., and Sakaba, T. (2009). Calcium dependence of exo- and endocytotic coupling at a glutamatergic synapse. Neuron *63*, 216–229.

Hua, Y., Sinha, R., Thiel, C.S., Schmidt, R., Hüve, J., Martens, H., Hell, S.W., Egner, A., and Klingauf, J. (2011). A readily retrievable pool of synaptic vesicles. Nat. Neurosci. *14*, 833–839.

Hua, Y., Woehler, A., Kahms, M., Haucke, V., Neher, E., and Klingauf, J. (2013). Blocking endocytosis enhances short-term synaptic depression under conditions of normal availability of vesicles. Neuron *80*, 343–349.

Jahn, R., and Scheller, R.H. (2006). SNAREs–engines for membrane fusion. Nat. Rev. Mol. Cell Biol. *7*, 631–643.

Jouhou, H., Yamamoto, K., Homma, A., Hara, M., Kaneko, A., and Yamada, M. (2007). Depolarization of isolated horizontal cells of fish acidifies their immediate surrounding by activating V-ATPase. J. Physiol. *585*, 401–412.

Kawasaki, F., and Ordway, R.W. (2009). Molecular mechanisms determining conserved properties of short-term synaptic depression revealed in NSF and SNAP-25 conditional mutants. Proc. Natl. Acad. Sci. USA *106*, 14658–14663.

Khvotchev, M.V., and Südhof, T.C. (2004). Stimulus-dependent dynamic homo- and heteromultimerization of synaptobrevin/VAMP and synaptophysin. Biochemistry *43*, 15037–15043.

Koo, S.J., Markovic, S., Puchkov, D., Mahrenholz, C.C., Beceren-Braun, F., Maritzen, T., Dernedde, J., Volkmer, R., Oschkinat, H., and Haucke, V. (2011). SNARE motif-mediated sorting of synaptobrevin by the endocytic adaptors clathrin assembly lymphoid myeloid leukemia (CALM) and AP180 at synapses. Proc. Natl. Acad. Sci. USA *108*, 13540–13545.

Kroch, A.E., and Fleming, K.G. (2006). Alternate interfaces may mediate homomeric and heteromeric assembly in the transmembrane domains of SNARE proteins. J. Mol. Biol. *357*, 184–194.

Kuner, T., Li, Y., Gee, K.R., Bonewald, L.F., and Augustine, G.J. (2008). Photolysis of a caged peptide reveals rapid action of N-ethylmaleimide sensitive factor before neurotransmitter release. Proc. Natl. Acad. Sci. USA *105*, 347–352.

Kwon, S.E., and Chapman, E.R. (2011). Synaptophysin regulates the kinetics of synaptic vesicle endocytosis in central neurons. Neuron *70*, 847–854.

Laage, R., and Langosch, D. (1997). Dimerization of the synaptic vesicle protein synaptobrevin (vesicle-associated membrane protein) II depends on specific residues within the transmembrane segment. Eur. J. Biochem. *249*, 540–546.

Lee, S.H., Shin, J.Y., Lee, A., and Bustamante, C. (2012). Counting single photoactivatable fluorescent molecules by photoactivated localization microscopy (PALM). Proc. Natl. Acad. Sci. USA *109*, 17436–17441.

Li, Z., Burrone, J., Tyler, W.J., Hartman, K.N., Albeanu, D.F., and Murthy, V.N. (2005). Synaptic vesicle recycling studied in transgenic mice expressing synaptopHluorin. Proc. Natl. Acad. Sci. USA *102*, 6131–6136.

McMahon, H.T., Bolshakov, V.Y., Janz, R., Hammer, R.E., Siegelbaum, S.A., and Südhof, T.C. (1996). Synaptophysin, a major synaptic vesicle protein, is not essential for neurotransmitter release. Proc. Natl. Acad. Sci. USA *93*, 4760–4764.

Miesenböck, G., De Angelis, D.A., and Rothman, J.E. (1998). Visualizing secretion and synaptic transmission with pH-sensitive green fluorescent proteins. Nature *394*, 192–195.

Mohrmann, R., de Wit, H., Verhage, M., Neher, E., and Sørensen, J.B. (2010). Fast vesicle fusion in living cells requires at least three SNARE complexes. Science *330*, 502–505.

Neher, E. (2010). What is Rate-Limiting during Sustained Synaptic Activity: Vesicle Supply or the Availability of Release Sites. Front. Synaptic Neurosci. *2*, 144.

Pennuto, M., Bonanomi, D., Benfenati, F., and Valtorta, F. (2003). Synaptophysin I controls the targeting of VAMP2/synaptobrevin II to synaptic vesicles. Mol. Biol. Cell *14*, 4909–4919.

Renz, M., Daniels, B.R., Vámosi, G., Arias, I.M., and Lippincott-Schwartz, J. (2012). Plasticity of the asialoglycoprotein receptor deciphered by ensemble FRET imaging and single-molecule counting PALM imaging. Proc. Natl. Acad. Sci. USA *109*, E2989–E2997.

Roy, R., Laage, R., and Langosch, D. (2004). Synaptobrevin transmembrane domain dimerization-revisited. Biochemistry *43*, 4964–4970.

Sakaba, T., and Neher, E. (2003). Involvement of actin polymerization in vesicle recruitment at the calyx of Held synapse. J. Neurosci. *23*, 837–846.

Saminathan, R., Pachiappan, A., Feng, L., Rowan, E.G., and Gopalakrishnakone, P. (2009). Transcriptome profiling of neuronal model cell PC12 from rat pheochromocytoma. Cell. Mol. Neurobiol. *29*, 533–548.

Schmitt, U., Tanimoto, N., Seeliger, M., Schaeffel, F., and Leube, R.E. (2009). Detection of behavioral alterations and learning deficits in mice lacking synaptophysin. Neuroscience *162*, 234–243.

Schoch, S., Deák, F., Königstorfer, A., Mozhayeva, M., Sara, Y., Südhof, T.C., and Kavalali, E.T. (2001). SNARE function analyzed in synaptobrevin/VAMP knockout mice. Science *294*, 1117–1122.

Sieber, J.J., Willig, K.I., Kutzner, C., Gerding-Reimers, C., Harke, B., Donnert, G., Rammner, B., Eggeling, C., Hell, S.W., Grubmüller, H., and Lang, T. (2007). Anatomy and dynamics of a supramolecular membrane protein cluster. Science *317*, 1072–1076.

Singec, I., Knoth, R., Ditter, M., Hagemeyer, C.E., Rosenbrock, H., Frotscher, M., and Volk, B. (2002). Synaptic vesicle protein synaptoporin is differently expressed by subpopulations of mouse hippocampal neurons. J. Comp. Neurol. *452*, 139–153.

Sinha, R., Ahmed, S., Jahn, R., and Klingauf, J. (2011). Two synaptobrevin molecules are sufficient for vesicle fusion in central nervous system synapses. Proc. Natl. Acad. Sci. USA *108*, 14318–14323.

Söllner, T., Whiteheart, S.W., Brunner, M., Erdjument-Bromage, H., Geromanos, S., Tempst, P., and Rothman, J.E. (1993a). SNAP receptors implicated in vesicle targeting and fusion. Nature *362*, 318–324.

Söllner, T., Bennett, M.K., Whiteheart, S.W., Scheller, R.H., and Rothman, J.E. (1993b). A protein assembly-disassembly pathway in vitro that may correspond to sequential steps of synaptic vesicle docking, activation, and fusion. Cell *75*, 409–418.

Spiwoks-Becker, I., Vollrath, L., Seeliger, M.W., Jaissle, G., Eshkind, L.G., and Leube, R.E. (2001). Synaptic vesicle alterations in rod photoreceptors of synaptophysin-deficient mice. Neuroscience *107*, 127–142.

Stevens, R.J., Akbergenova, Y., Jorquera, R.A., and Littleton, J.T. (2012). Abnormal synaptic vesicle biogenesis in Drosophila synaptogyrin mutants. J. Neurosci. *32*, 18054–18067, 18067a.

Takamori, S., Holt, M., Stenius, K., Lemke, E.A., Grønborg, M., Riedel, D., Urlaub, H., Schenck, S., Brügger, B., Ringler, P., et al. (2006). Molecular anatomy of a trafficking organelle. Cell *127*, 831–846.

Threadgill, R., Bobb, K., and Ghosh, A. (1997). Regulation of dendritic growth and remodeling by Rho, Rac, and Cdc42. Neuron *19*, 625–634.

van den Bogaart, G., Holt, M.G., Bunt, G., Riedel, D., Wouters, F.S., and Jahn, R. (2010). One SNARE complex is sufficient for membrane fusion. Nat. Struct. Mol. Biol. *17*, 358–364.

Washbourne, P., Schiavo, G., and Montecucco, C. (1995). Vesicle-associated membrane protein-2 (synaptobrevin-2) forms a complex with synaptophysin. Biochem. J. *305*, 721–724.

Wienisch, M., and Klingauf, J. (2006). Vesicular proteins exocytosed and subsequently retrieved by compensatory endocytosis are nonidentical. Nat. Neurosci. *9*, 1019–1027.

Wu, X.S., McNeil, B.D., Xu, J., Fan, J., Xue, L., Melicoff, E., Adachi, R., Bai, L., and Wu, L.G. (2009). Ca(2+) and calmodulin initiate all forms of endocytosis during depolarization at a nerve terminal. Nat. Neurosci. *12*, 1003–1010.

Xu, T., Ashery, U., Burgoyne, R.D., and Neher, E. (1999). Early requirement for alpha-SNAP and NSF in the secretory cascade in chromaffin cells. EMBO J. *18*, 3293–3304.